Molecular Level One-Step Activation of agar to Activated Carbon for High Performance Supercapacitors

Lixing Zhang [a], Huazhi Gu [a], Haibo Sun [a], Feifei Cao [d], Yao Chen [a,*] and George Zheng Chen [a,b,c]

[a] The State Key Laboratory of Refractories and Metallurgy, College of Materials and Metallurgy, Wuhan University of Science and Technology, Wuhan 430081, P. R. China.

[b] Department of Chemical and Environmental Engineering, Faculty of Science and Engineering, University of Nottingham Ningbo China, Ningbo 315100, P. R. China

[c] Department of Chemical and Environmental Engineering, Faculty of Engineering, University of Nottingham, Nottingham NG2 7RD, UK

[d] College of Science, Huazhong Agricultural University, No.1 Shizishan Street, Hongshan District, Wuhan, 430070, P. R. China

[*] Corresponding author.

E-mail address: y.chen@wust.edu.cn (Y. Chen).

Abstract

Activated carbon was synthesized by a simple one-step calcination of deoxygenated agar in a hot KOH aqueous solution, in which KOH plays both deoxidant and activation agent. The deoxygenation course omits high temperature carbonization in the conventional technology and leads to molecular level activation of agar in subsequent one-step calcination. The one-step activated carbon has superior specific surface area of 1672 m^2 g^{-1} and total pore volume of 0.81 cm^3 g^{-1}. It also shows a maximum specific capacitance of 226 F g^{-1} in the KOH electrolyte, which is 1.4 times as high as that for the activated carbon by the conventional two-step method. This study provides potentially economical and effective means for the production of commercial activated carbon with high porosity for supercapacitors.

1. Introduction

Because traditional fossil fuels which cause environmental pollution and global climate warming are limited, searching for green energy and new energy storage devices is imminent. Supercapacitors are one type of the most important energy storage devices, which show higher power and longer lifetime comparing with second batteries [1-3]. Intrinsic supercapacitors are based on electrochemical double layer (EDL) capacitance mechanism that store and release energy by charge separation at the interface between an electrode and an electrolyte. Various carbon materials have been used in the electrodes of EDL capacitors, including activated carbon, carbon nanotubes and graphene [4-10]. Meanwhile, transition metal oxides and conductive polymers are employed as the electrode materials for pseudocapacitors based on the other Faradic reaction mechanism. Comparing with these pseudocapacitance materials, carbon materials possess absolute advantages in high power and lifetime except relative low specific capacitance [11-13]. Additionally, pseudocapacitance materials also shows low specific capacitance in ionic liquid, for example, MnO_2 has a specific capacitance of 100 F g^{-1} in doped Butylmethylpyrrolidinium–dicyanamide with 3 V of potential window [14]. Therefore, the development of carbon materials toward the desire of high specific capacitance has been arousing widespread interest in supercapacitors.

Among all carbon materials, activated carbon is the earliest commercial electrode of supercapacitors due to its porous structures with large specific surface area, good electrical conductivity, excellent physical, chemical and electrochemical

stability and low cost [15-20]. In the conventional approach, a two-step process composed of carbonization and subsequent activation of carbon rich precursors is usually applied to prepare activated carbon. While these carbon based supercapacitors demonstrate excellent properties, the two-step technology reducing high cost per kWh has limited the competition of supercapacitors with lithium-ion batteries in many applications [21]. Hence it is necessary to increase the capacitance of carbon electrodes using a more simple and effective approach in the electrode processing currently used in the manufacture of supercapacitors. Up to date, only two reports on one-step calcination of the mechanical mixture of biomass or agar and KOH have executed activation with similar yield and properties compared with those that are prepared via the conventional two-step route [22,23].

Herein, we report on a novel approach to fabricate activated carbon via one-step calcination of deoxygenated agar via hot KOH aqueous solution. KOH which is homogeneously mixed with agar in the hot solution by a soft chemical method plays both deoxidant and activation agent, which omits high temperature carbonization in the conventional technology and leads to molecular level activation of agar in subsequent one-step calcination. The deoxygenation mechanism of agar in the hot KOH solution before the one-step calcination is also revealed for the first time. The activated carbon by one-step method shows a specific surface area of 1672 m^2 g^{-1}, much higher than 1048 m^2 g^{-1} for the activated carbon by conventional two-step method. As a result, the activated carbon by one-step method shows 226 F g^{-1} at 1 A g^{-1} in 6 M KOH aqueous solution, 1.4 times as high as the activated carbon by

two-step method.

2. Experimental

2.1. Preparation of samples

4.5 g KOH and a 5 g agar were dissolved in distilled (DI) water in a water bath at 95 ^{o}C. A black hydrogel was obtained when the reaction finished. After thorough drying, the dried hydrogel was conducted at 725 ^{o}C for 1 h in Ar. Finally, the activated carbon was obtained by washing with 15% HCl, abundant water for 5 times, and dried at 80 ^{o}C for 12 h, which is denoted as AC-1. For comparison, activated carbon was also prepared via a conventional two-step process composing of carbonization of 5 g agar at 725 ^{o}C for 1 h and subsequent activation with 4.5 g KOH at 725 ^{o}C for 1 h, which is named as AC-2.

2.2. Characterization of samples

The X-ray photoelectron spectroscope (XPS) spectra were recorded on 250XI (ThermoFisher). The metal contents of the composite were analyzed using ICP-OES on IRIS Advantage ER/S (Thermo Elemental). The morphology and elemental content were obtained by scanning electron microscopy (SEM, FEI Nova 400 Nano SEM) with X-ray energy disperse spectrum (EDS). Transmission electron microscopy (TEM) morphology was investigated by JEOL JSM 2100F. A Fourier-transform Infrared (FTIR) spectrometer (Shimadzu Spectrum One FTIR) was used to analyze the change of functional groups of the precursor. The N_2 adsorption/desorption isotherms were obtained at 77 K using automatic volumetric

adsorption equipment (ASAP2020HD88).

2.3. Electrochemical measurements

A mixture of activated carbon, acetylene black and polyvinylidene difluoride with a weight ratio of 8:1:1 was pasted on nickel substrates as a working electrode with a surface density of 0.45 mg cm^{-2}. For the three-electrode tests, a platinum foil and a Hg/HgO electrode or two platinum foils were used as counter and reference electrodes in 6 M KOH or pure 1-ethyl-3-methyl-imidazolium tetrafluoroborate ($EMIMBF_4$) as electrolytes. For the full cell tests, the activated carbon mixtures on the nickel substrates were assembled to coin-type symmetrical SCs in ambient or an Ar glove box (MIKROUNA) for electrolytes of 6 M KOH or pure 1-ethyl-3-methyl-imidazolium tetrafluoroborate ($EMIMBF_4$). Cyclic voltammetry (CV), galvanostatic charge/discharge (GCD) and electrochemical impedances spectroscopy (EIS) were measured by a CHI 660E electrochemical workstation and the cyclic performances were measured by a LAND CT2001A system.

3. Results and discussion

Activated carbons are usually derived from organic precursors by carbonization at high temperature with subsequent selective oxidation with KOH to increase the SSA and pore volume in inert atmosphere. Intrinsically, the carbonization at high temperature is a deoxygenation course of the organic precursors in order to prevent from burning out of them in subsequent KOH activation. Agar, consisting of agarose and agaropectin, is an organics with a C/O atomic ratio of 1.34. When agar was mixed

with hot alkaline aqueous solution, it is found that the aqueous solution turned dark after a few minutes. In order to verify the reaction between agar and KOH, the resulted dark agar gel, named D-agar, in the hot alkaline aqueous solution was separated by dialysis to remove extra KOH. The ICP-AES analysis of D-agar reveals that the content of K is 2.61 wt%, indicative of no O–K bond in D-agar. The EDS spectra of D-agar reveal that an average C/O atomic ratio of 3.45±0.70, which is much higher than 1.34 for agar. The increased C/O atomic ratio indicates that the agar was deoxidized in hot KOH aqueous solution. The FTIR spectra of agar and D-agar in Fig. 1 reveal the molecular structural change of agar in the reaction. Both spectra of agar and D-agar show two small adsorption peaks at 1654 and 2890 cm^{-1}, which are ascribed to carbonyl (C=O) from agaropectin in agar and C–H stretching and bending vibrations. These bonds can not readily react with KOH. The decreased intensities of the broad absorption band at 3300~3600 cm^{-1} and the peak at 1075 cm^{-1} are obviously observed for D-agar, suggesting that the hydrogen bonded hydroxyl groups and cyclic ether linkage of six membered rings in agar are removed by a dehydration reaction with KOH in the hot solution [24,25]. The elimination of oxygen functional groups can replace the carbonization step in the conventional two-step method and ensure a yield of 2.7 % for activated carbon with a tapping density of 0.18 g cm^{-3}. However, the yield for one-step derived AC-1 is still much lower than 16.2 % for AC-2 with a tapping density of 0.46 g cm^{-3}. Further, the average carbon and oxygen contents of AC-1 are determined to be 91.21 and 8.79 at% by EDS. The XPS spectrum of AC-1 shows a small peak at 286.1 eV, corresponding to C–O bond (Fig.

S1), while its FTIR spectrum exhibits a characteristic C–O bond at 1220 cm^{-1} (Fig. S2), suggesting that oxygen in AC-1 is in the form of C–O bond.

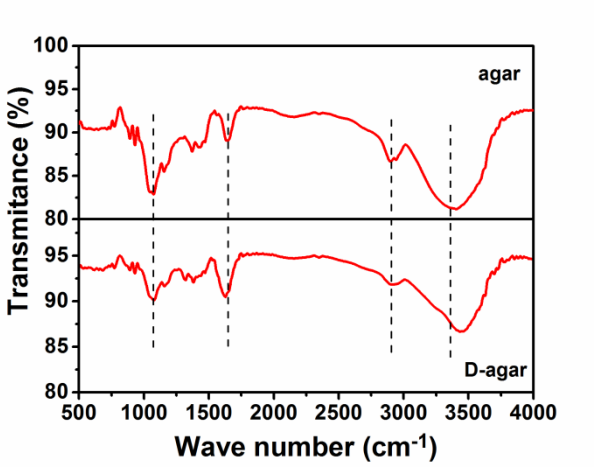

Fig. 1 FTIR spectra of agar and D-agar.

The morphologies of AC-1 and AC-2 were observed by SEM and TEM. The SEM image of AC-1 in low and high magnification (Fig. 2a and b) show that an interconnected 3D network with macrovoids of several micrometers and their wall of a few hundreds of nanometers. The TEM image of AC-1 in Fig. 2d shows the dense micropores which are less than 1 nm. AC-2 presents bulk characteristic with size of above 30 μm composed of fractured macrovoids of tens of micrometers in Fig. 2c, which is one order of magnitude higher than that of AC-1. The retainence of the interconnected structure with smaller size for AC-1 are obviously attributed to a mild deoxygenation of agar instead of carbonization at high temperature.

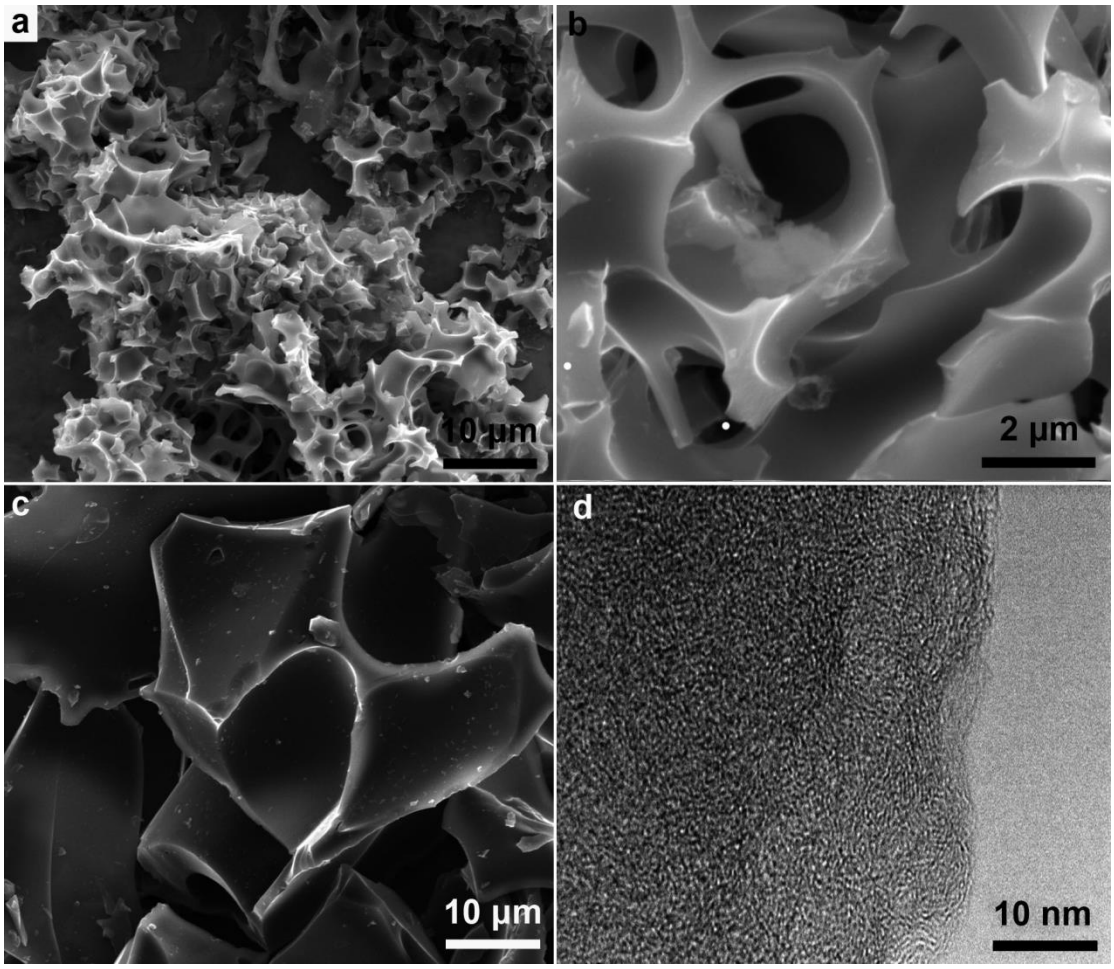

Fig. 2 (a) Low and (b) High magnification SEM images of AC-1. (c) Low magnification SEM image of AC-2. (d) High resolution TEM image of AC-1.

The adsorption and desorption isotherms of N_2 at 77 K and the pore size distribution of AC-1 and AC-2 are shown in Fig. 3. Obviously, all the samples exhibiting a type I nitrogen adsorption desorption isotherms in the Brunauer classification [26] confirms their microporous structure (Fig. 3a), well consistent with the TEM observations. Although AC-1 and AC-2 have almost similar pore size distributions mainly ranging from 0.5 to 3 nm (Fig. 3b), AC-1 possesses a larger specific surface area of 1672 $m^2 g^{-1}$ and total pore volume of 0.81 $cm^3 g^{-1}$ than 1048

$m^2 g^{-1}$ and 0.47 $cm^3 g^{-1}$ for AC-2, respectively.

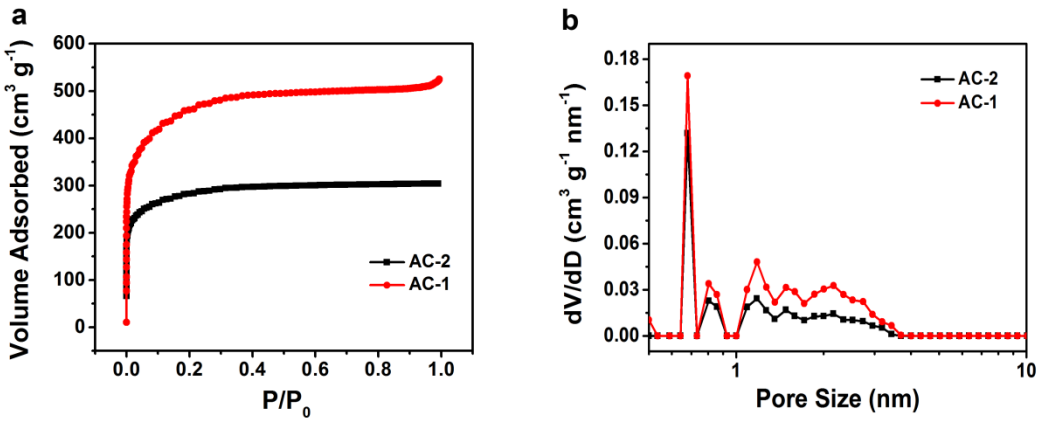

Fig. 3 (a) nitrogen adsorption-desorption isotherms and (b) pore size distribution plot of AC-1 and AC-2.

The electrochemical properties of AC-1 and AC-2 were estimated by cyclic voltammetry (CV) and galvanostatic charge/discharge (GCD) measurements using a three-electrode cell in the potential range from 0 to –1 V in 6 M KOH eletrolyte. Fig. 4a features their CV curves at a scan rate of 10 mV s^{-1}. These CV profiles are quasi-rectangular in shape without obvious redox peaks, indicating that both samples have ideal capacitive behavior. However, the larger area of CV curves for the AC-1 electrode means higher specific capacitance than that of the AC-2 electrodes due to its higher specific surface area and well-developed porous structure which accommodate more electrolyte ions. Fig. 4b exhibits the GCD curves of AC-1 and AC-2. As revealed by Fig. S3, the discharge curve in a three-electrode cell within the whole potential window includes a discharge curve within relative positive potential window and a charge curve within relative negative potential window, so it is possible that the charge time is less than the discharge time in a three-electrode cell. Considering that

columbic efficiency should not be beyond 100 %, the specific capacitance of AC-1 is calculated from the charging curves to be 226 F g^{-1} at a specific current of 1 A g^{-1}. It is 38 % higher than 164 F g^{-1} of AC-2 at the same specific current. All CV profiles of AC-1 retain a rectangular shape at different sweep rates (Fig. 4c). No obvious distortion in the CV curves at 200 mV s^{-1} indicates an excellent rate capability due to low equivalent series resistance and the fast diffusion of electrolyte ions into the electrode. According to Fig. 4d, the capacitance of AC-1 only decreases to 208 F g^{-1} at 10A g^{-1}, having a superb capacitive retention of 92% relative to 226 F g^{-1} at 1 A g^{-1}.

Compared with AC-2, the electrochemical performances of AC-1 are evidently improved. The effective execution of the one-step method mainly relies on the deoxygenation course in the hot KOH solution which can increase the carbon yield. Alternatively, the deoxygenation course in one-step method extends the selection of precursors from rich carbon ones to ones with many oxygen functional groups. The deoxygenation course requires the solubility and reactive functional groups of the precursor. The high solubility of agar in hot water ensure the homogeneous deoxygenation itself with KOH, which further leads to molecular level distribution of KOH in D-agar. Conversely, insoluble polyaniline without reactive functional groups via the one-step method always produces gray powders. The uniformed activation of agar produces interconnected 3D network with small size macrovoids, also meaning that more pores are produced in more external surface. As a result, larger capacitance is obtained in AC-1 by the one-step method.

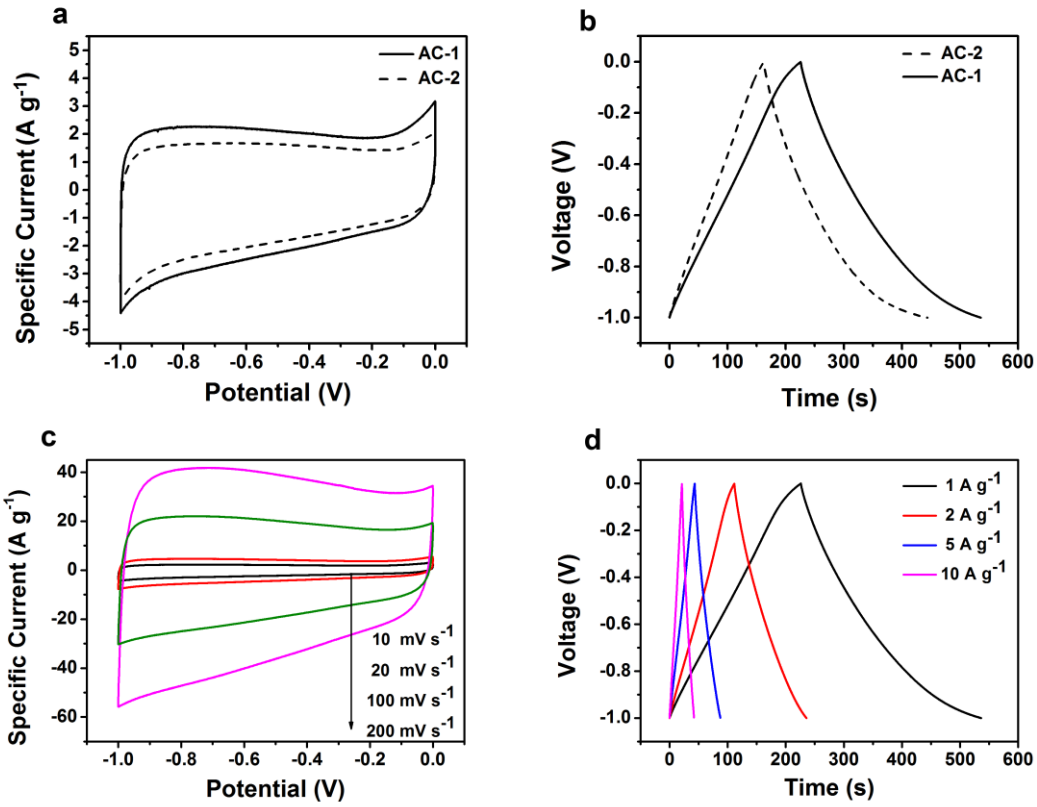

Fig. 4 Three-electrode electrochemical performances in 6 M KOH. (a) CV curves of AC-1 and AC-2 at 10 mV s^{-1}. (b) GCD curves of AC-1 and AC-2 at 1A g^{-1}. (c) CV curves of AC-1 at different scan rates in 6 M KOH solution. The arrow indicates the increase of the scan rates from 10 to 200 mV s^{-1}. (d) GCD curves of AC-1 at different specific currents from 1 to 10 A g^{-1}.

Symmetrical two-electrode coin type supercapacitors were constructed using both aqueous (6 M KOH) and ionic liquids ($EMIMBF_4$) as electrolytes. The nearly rectangular CV profiles and the symmetrical triangular charge/discharge plots are well maintained at different scan rates and specific currents within the potential window of 1 V using 6 M KOH electrolyte (Fig. 5 and S4), indicating that the EDL mechanism

dominates the electrochemical behavior of AC-1 for the aqueous supercapacitors. The maximum specific capacitance of the symmetrical AC-1 cell is 57 F g^{-1} with surface density of 0.45 mg cm^{-2} at 0.25 A g^{-1} according to the discharge curves, corresponding to 228 F g^{-1} for a single electrode, which is consistent with the value in the three-electrode cell. The coulombic and energy efficiencies are 92.7% and 73.1% in KOH electrolyte, respectively. To evaluate the performance for practical application, the AC-1 electrode with surface density of 10 mg cm^{-2} has been loaded on nickel foams. Even with such a large mass loading, the AC-1 electrode still shows a specific capacitance of 46 F g^{-1} at 0.25 A g^{-1}. When $EMIMBF_4$ was employed as electrolyte instead of KOH, it is found that the threshold potentials of ionic liquid decomposition and carbon oxidation for AC-1 in the ionic liquid electrolyte are −1.9 and 0.9 V vs. Pt in a three-electrode cell, giving a stable electrochemical window of 2.8 V, as shown in Fig. S5 [27,28]. The EIS method also has been used to analyze the potential window in the three electrode cell in $EMIMBF_4$. According to Fig S6, the shapes of the Nyquist plots in low frequency obviously deviate from a vertical line when the voltage range exceeds −1.9 to 0.9 V. The phase angles in Fig. S7 for −2 and 1 V of the initial potentials are both below -40°, which is far from -90° corresponding to an ideal capacitive characteristic [29]. The CV measurements of the AC-1 cell in the $EMIMBF_4$ electrolyte also shows rectangular profiles with potential window of 2.8 V at different scan rates in Fig. 6a. The highest specific capacitance of the AC-1 cell in the $EMIMBF_4$ electrolyte is calculated to be 17 F g^{-1} with surface density of 0.45 mg cm^{-2} and 16 F g^{-1} with surface density of 10 mg cm^{-2} at 0.25 A g^{-1} by the

discharge curves in the GCD process (Fig 6b, c and S8), corresponding to a specific capacitance of 68 F g^{-1} for a single electrode. The coulombic and energy efficiencies are 87.8% and 60.1% in $EMIMBF_4$ electrolyte, respectively, which are lower than those in KOH, indicating low reversibility wihin 2.8 V in $EMIMBF_4$ [30,31]. The specific energy of AC-1 in the cell is calculated to be 18.5 Wh kg^{-1} for the cell.

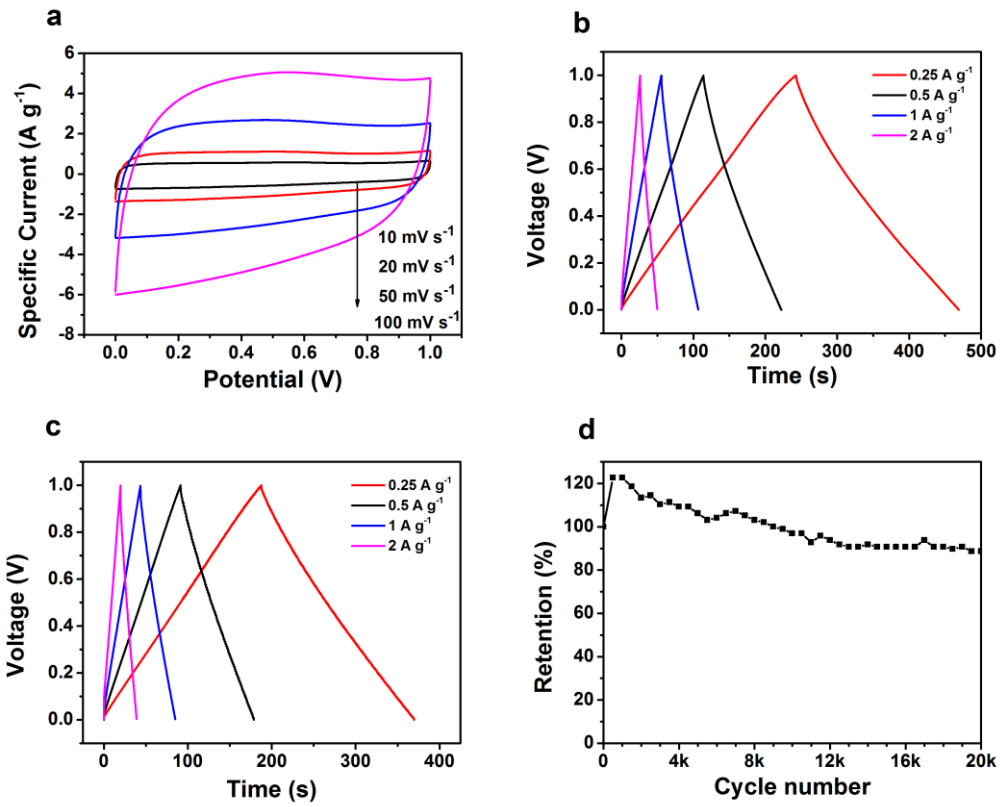

Fig. 5 Two-electrode electrochemical performances of the AC-1 cell in 6 M KOH. (a) CV curves at different scan rates, the arrow indicates the increase of the scan rates from 10 to 100 mV s^{-1}. (b) GCD curves at different specific currents with the surface density of 0.45 mg cm^{-2} on the nickel foils and (c) the surface density of 10 mg cm^{-2} on the nickel foams. (d) Cyclic performance of AC-1 in KOH at 1A g^{-1}.

The cyclic performances of AC-1 in KOH and $EMIMBF_4$ at room temperature are present in Fig. 5d, 6d and S9. 88.6 and 63.6 % of the initial capacitance can be retained for AC-1 in the 6 M KOH and $EMIMBF_4$ electrolytes at 1 A g^{-1} after the 20000 and 3000 cycles, respectively. Interestingly, the AC-1 cell using KOH as electrolyte shows a progressive increase in the specific capacitance before 1000 cycles, which is attributed to better wetting at the electrolyte/electrode interface, especially in deep pores, after cycles [2,32-34]. In case of $EMIMBF_4$, after 500 cycles, the AC-1 only maintains 80% of the initial capacitance. The rapid deterioration and relative narrow potential window in $EMIMBF_4$ are attributed to the irreversible redox reaction arising from 8.79 at% C–O bond in AC-1 [35-37]. However, it is believed that very low oxygen content in carbon also can be realized by the new one-step method.

4. Conclusions

Activated carbon was synthesized by a simple one-step calcination of deoxygenated agar in a hot KOH aqueous solution. The deoxygenation course of soluble agar in the hot KOH solution omits high temperature carbonization in the conventional technology and leads to molecular level activation of agar in subsequent one-step calcination. The one-step activated carbon (AC-1) has superior specific surface area of 1672 m^2 g^{-1} and total pore volume of 0.81 cm^3 g^{-1}, obviously higher than those of the activated carbon by the conventional two-step method (AC-2). As a result, the

maximum specific capacitance of 226 F g^{-1} in the KOH electrolyte is obtained for AC-1 is higher than 164 F g^{-1} for AC-2. However, AC-1 also shows a rapid deterioration and relative narrow potential window in $EMIMBF_4$ due to 8.79 at% C–O bond in AC-1. This study provides potentially economical and effective means for the production of commercial activated carbon with high porosity for supercapacitors.

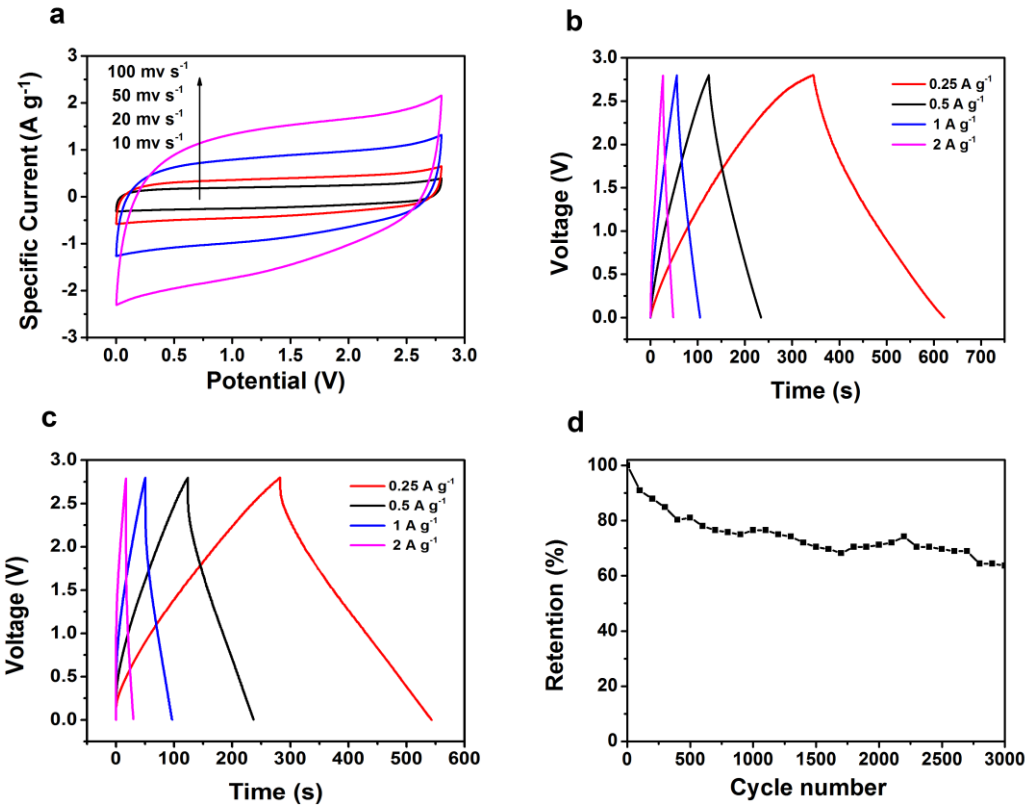

Fig. 6 Two-electrode electrochemical performances of the AC-1 cell in $EMIMBF_4$. (a) CV curves at different scan rates, the arrow indicates the increase of the scan rates from 10 to 100 mV s^{-1}. (b) GCD curves at different specific currents with the surface density of 0.45 mg cm^{-2} on the nickel foils and (c) the surface density of 10 mg cm^{-2} on the nickel foams. (d) Cyclic performance of AC-1 in $EMIMBF_4$ at 1A g^{-1}.

Acknowledgement

This work was partially supported by the financial support from the Department of Education of Hubei Provincial People's Government (Scientific Research Program, Q20161104).

References

[1] Chen GZ. Supercapacitor and supercapattery as emerging electrochemical energy stores. Inter Mater Rev 2017;62:173-202.

[2] González A, Goikolea E, Andoni Barrena J, Mysyk R. Review on supercapacitors: technologies and materials. Renew Sust Energy Rev 2016;58:1189-206.

[3] Chen HY, Zeng S, Chen MH, Zhang YY, Li QW. Fabrication and functionalization of carbon nanotube films for high-performance flexible supercapacitors. Carbon 2015;92:271-96.

[4] Gromadskyi DG, Chae JH, Norman SA, Chen GZ. Correlation of energy storage performance of supercapacitor with iso-propanol improved wettability of aqueous electrolyte on activated carbon electrodes of various apparent densities. App Energy 2015;159:39-50.

[5] Zhu YW, Murali S, Stoller MD, Ganesh KJ, Cai WW, Ferreira PJ, et al. Carbon-based supercapacitors produced by activation of graphene. Science 2011;332:1537-40.

[6] Zheng C, Zhou XF, Cao HL, Wang GH, Liu ZP. Synthesis of porous graphene/activated carbon composite with high packing density and large specific surface area for supercapacitor electrode material. J Power Sources 2014;258:290-6.

[7] Gao S, Wang K, Du ZL, Wang YL, Yuan AB, Lu W, et al. High power density electric double-layer capacitor based on a porous multi-walled carbon nanotube

microsphere as a local electrolyte micro-reservoir. Carbon 2015;92:254-61.

[8] Chen Y, Zhang X, Zhang DC, Yu P, Ma YW. High performance supercapacitors based on reduced graphene oxide in aqueous and ionic liquid electrolytes. Carbon 2010;49:573-80.

[9] Wu SL, Chen GX, Kim NY, Zhu YW. Creating pores on graphene platelets by low-temperature KOH activation for enhanced electrochemical performance. Small 2012;12:2376-84.

[10] Wei XJ, Zou HL, Gao SY. Chemical crosslinking engineered nitrogen-doped carbon aerogels from polyaniline-boric acid-polyvinyl alcohol gels for high performance electrochemical capacitors. Carbon 2017;123:471-80.

[11] Karnan M, Subramani K, Srividhy PK, Sathish M. Electrochemical studies on corncob derived activated porous carbon for supercapacitors application in aqueous and non-aqueous electrolytes. Electrochim Acta 2017;228:586-96.

[12] Tooming T, T. Thomberg, H. Kurig, Janes A, Lust E. High power density supercapacitors based on the carbon dioxide activated D-glucose derived carbon electrodes and 1-ethyl-3-methylimidazolium tetrafluoroborate ionic liquid. J Power Sources 2015;280: 667-77.

[13] Li X, Wei BQ. Supercapacitors based on nanostructured carbon. Nano Energy 2013:2:159-173.

[14] Li YS, Sun IW, Chang JK, Sua CJ. Doped butylmethylpyrrolidinium-dicyanamide ionic liquid as an electrolyte for MnO_2 supercapacitors. J Mater Chem 2012;22:6274-9.

[15] Sun W, Lipka SM, Swartz C, William D, Yang FQ. Hemp-derived activated carbons for supercapacitors. Carbon 2016;103:181-92.

[16] Chae JH, Chen GZ. 1.9 V aqueous carbon–carbon supercapacitors with unequal electrode capacitances. Electrochim Acta 2012;86:248-54.

[17] Zhang DD, Zhao JH, Feng C, Zhang JJ. Scalable synthesis of hierarchical macropore-rich activated carbon microspheres assembled by carbon nanoparticles for high rate performance supercapacitors. J Power Sources 2017;342:363-70.

[18] Wei L, Sevilla M, Fuertes AB, Mokaya R, Yushin G. Polypyrrole-derived activated carbons for high-performance electrical double-layer capacitors with ionic liquid electrolyte. Adv Func Mater 2012;22:827-34.

[19] Díez N, Mysyk R, Zhang W, Goikolea E, Carriazo D. One-pot synthesis of highly activated carbons from melamine and terephthaldehyde as electrodes for high energy aqueous supercapacitors. J Mater Chem A 2017;5:14619-29.

[20] Tian X, Ma HR, Li Z, Yan SC, Ma L, Yu F, et al. Flute type micropores activated carbon from cotton stalk for high performance supercapacitors. J Power Sources 2017;359: 88-96.

[21] Hwang JY, Li MP, El-Kady MF, Kaner RB. Next-generation activated carbon supercapacitors: a simple step in electrode processing leads to remarkable gains in energy density. Adv Funct Mater 2017;27:1605745.

[22] Rehman S, Gu XX, Khan K, Mahmood N, Hou YL, Huang XX, et al. 3D vertically aligned and interconnected porous carbon nanosheets as sulfur

immobilizers for high performance lithium-sulfur batteries. Adv Energy Mater 2016;6:1502518.

[23] Balahmar N, Al-Jumialy AS, Mokaya R. Biomass to porous carbon in one step: directly activated biomass for high performance CO_2 storage. J Mater Chem A 2017;10:1039.

[24] Laksaci H, Khelifi A, Trari M, Addoun A. Synthesis and characterization of microporous activated carbon from coffee grounds using potassium hydroxides. J Clean Prod 2017;147:254-62.

[25] Li M, Li W, Liu SX. Hydrothermal synthesis, characterization, and KOH activation of carbon spheres from glucose. Carbohyd Res 2011;346:999-1004.

[26] Brunauer S, Emmett P, Teller E. Adsorption of gases in multimolecular layers. J Am Chem Soc 1938;60:309.

[27] Li J, Tang J , Yuan JS, Zhang K, Shao QG, Qin LC, et al. Interactions between graphene and ionic liquid electrolyte in supercapacitors. Electrochim Acta 2016;197:64-91.

[28] Lewandowski A, Olejniczak A, Galinski M, Stepniak I. Performance of carbon-carbon supercapacitors based on organic, aqueous and ionic liquid electrolytes. J Power Sources 2010;195:5814-9.

[29] Härmas M, Thomberg T, Romann T, Jänes A, Lust E. Carbon for energy storage derived from granulated white sugar by hydrothermal carbonization and subsequent zinc chloride activation. J Electrochem Soc 2017;164: A1866-72.

[30] Weingarth D, Foelske-Schmitz A, Kötz R. Cycle versus voltage hold – Which is

the better stability test for electrochemical double layer capacitors. J Power Sources 2013;225:84-8.

[31] Kötz R, Carlen M. Principles and applications of electrochemical capacitors. Electrochim Acta 2000;45:2483-98.

[32] Chen Y, Zhang X, Zhang HT, Sun XZ, Zhang DC, Ma YW. High-performance supercapacitors based on a graphene–activated carbon composite prepared by chemical activation. RSC Adv 2012;2:7747-53.

[33] Hahn M, Barbieri O, Gallay R, Kötz R. A dilatometric study of the voltage limitation of carbonaceous electrodes in aprotic EDLC type electrolytes by charge-induced strain. Carbon 2006;44:2523-33.

[34] Hastak RS, Sivaraman P, Potphode DD, Shashidhara K, Samui AB. All solid supercapacitor based on activated carbon and poly [2,5-benzimidazole] for high temperature application. Electrochim Acta 2012;59:296-303.

[35] Eskusson J, Jänes A, Kikas A, Matisen L, Lust E. Physical and electrochemical characteristics of supercapacitors based on carbide derived carbon electrodes in aqueous electrolytes. J Power Sources 2011;196:4109-16.

[36] Li SM, Yang SY, Wang YS, Tsai HP, Tien HW, Hsiao ST, Liao WH, Chang CL, Ma CCM, Hu CC. N-doped structures and surface functional groups of reduced graphene oxide and their effect on the electrochemical performance of supercapacitor with organic electrolyte. J Power Sources 2015;278:218-29.

[37] Tian WQ, Gao QM, Tan YL, Zhang YL, Xu JD, Li ZY, Yang K, Zhu LH, Liu ZP. Three-dimensional functionalized graphenes with systematical control over the

interconnected pores and surface functional groups for high energy performance supercapacitors. Carbon 2015;85:351-62.